Dual-atom Pt heterogeneous catalyst with excellent catalytic performances for the selective hydrogenation and epoxidation

Shubo Tian
Institute of Solid state physics
Zizhan He
Shandong University
Wanbing Gong
Institute of Solid State Physics
Qi Xu
Tsinghua University
Wenxing Chen
Beijing Institute of Technology
Youqi Zhu
Beijing Institute of Technology
Jiarui Yang
Tsinghua University
Qiang Fu (qfu@sdu.edu.cn)
Shandong University https://orcid.org/0000-0002-6682-8527
Chun Chen
Institute of Solid State Physics, Chinese Academy of Sciences
Yuxiang Bu
Shandong University https://orcid.org/0000-0002-6445-5069
Xiaoming Sun
Beijing University of Chemical Technology
Huijun Zhao
Institute of Solid State Physics
Dingsheng Wang (wangdingsheng@mail.tsinghua.edu.cn)
Tsinghua University https://orcid.org/0000-0003-0074-7633
Yadong Li
Tsinghua University

Article

Keywords: heterogeneous catalytic materials, wet-chemical, mesoporous graphitic carbon nitride (mpg-C3N4)

Posted Date: July 8th, 2020

DOI: https://doi.org/10.21203/rs.3.rs-38437/v1

Version of Record: A version of this preprint was published at Nature Communications on May 26th, 2021. See the published version at https://doi.org/10.1038/s41467-021-23517-x.

Abstract

Atomically monodispersed heterogeneous catalysts with uniform active sites and high atom utilization efficiency are ideal heterogeneous catalytic materials. Designing such type of catalysts, however, remains a formidable challenge. Herein, using a wet-chemical method, we successfully achieved a mesoporous graphitic carbon nitride (mpg-C3N4) supported dual-atom Pt2 catalyst, which exhibited excellent catalytic performance for the highly selective hydrogenation of nitrobenzene to aniline. The conversion of ≥99% is significantly superior to the corresponding values of mpg-C3N4-supported single Pt atoms and ultra-small Pt nanoparticles. First-principles calculations revealed that the excellent performance of the dual-atomic Pt2 species originates from an effective activation of the nitro groups in the reactant. The produced Pt2/mpg-C3N4 samples are versatile and can be applied in catalyzing other important reactions, such as the selective hydrogenation of benzaldehyde and the epoxidation of styrene.

Introduction

Atomically monodispersed heterogeneous catalysts with uniform active sites can be used as ideal models for understanding the correlations between compositions/structures and the corresponding performances, which are not only significant but also challenging in heterogeneous catalysis research.[1–4] Besides, atomically monodispersed catalysts also have high atom utilization efficiency and usually exhibit excellent catalytic activity.[5–9] The well-known single-atom catalysts have been widely employed in many heterogeneous reactions.[10–23] Compared with single-atom catalysts, dual-atom catalysts not only possess the same advantages of uniformity in the active sites and high atom utilization efficiency,[24–27] the two metal atoms involved can also cooperate and play a synergistic role in optimizing interactions between the active sites and reactants or intermediates.[28–33] This may help to break the intrinsic linear scaling relationship between adsorption energies of reaction intermediate and further improve the catalytic performances. Although dual-atom heterogeneous catalysts possess so many unique advantages, synthesizing such materials remains a great challenge, which mainly comes from the difficulty in controlling uniform configurations of the active sites at the atomic scale.

Selective hydrogenation and epoxidation are two significant approaches to produce fine chemicals and high-value products in practical industrial applications.[34–35] These reactions include, for instance, the selective hydrogenation of nitroarenes to amines[36–37], the selective hydrogenation of aldehyde compounds to alcohol compounds[38–39], and the epoxidation of alkenes to epoxides[40–41]. So far, many non-noble metal catalysts have been developed for catalyzing the reactions, but the harsh reaction conditions hinder their wide applications[42–43] Currently, conventional noble-metal catalysts are still the most commonly employed catalysts in those reactions, but they generally suffer from low atom utilization efficiency and the inevitably high cost.[41–44] We thereby expect atomically monodispersed heterogeneous catalysts to play a role in the reactions.

Herein, we have successfully synthesized a Pt_2/mpg-C_3N_4 catalyst by using a simple wet-chemical method. The as-prepared sample possessed a dual-atom Pt_2 structure that was evidenced with aberration correction transmission electron microscopy, X-ray absorption fine structure data, and first-principles simulations. The dual-atom Pt species exhibited excellent catalytic performance toward the selective hydrogenation of nitrobenzene to aniline and behaved much better than Pt single-atom catalysts and ultra-small Pt nanoparticles. First-principles calculations revealed that the unique catalytic properties of Pt_2/mpg-C_3N_4 originate from its ability to effectively activate the N = O bonds of the nitro groups. The application of the superior Pt_2/mpg-C_3N_4 catalyst has also been extended to the selective hydrogenation of benzaldehyde to benzyl alcohol and the epoxidation of styrene to styrene oxide.

Results

Synthesis and characterization of Pt_2/mpg-C_3N_4 samples. The Pt_2/mpg-C_3N_4 sample was synthesized using the wet-chemical strategy. (Ethylenediamine)iodoplatinum(II) dimer dinitrate and mesoporous graphitic carbon nitride (mpg-C_3N_4) were selected as the dual-atomic Pt precursor and the substrate. They were mixed and further pyrolyzed to remove the ligands from the dual-atom Pt precursor. The Pt_1/mpg-C_3N_4 and the Pt nanoparticle/mpg-C_3N_4 samples were synthesized using the same method, except the Pt species being replaced by H_2PtCl_6 and Pt nanoparticles, respectively.

The X-ray diffraction (XRD) pattern (Supplementary Fig. S1) demonstrated that the synthesized mpg-C_3N_4 sample has a graphitic packing structure,[45,46] and the disordered spherical pores of mpg-C_3N_4 were captured by the transmission electron microscopy (TEM) image (Supplementary Fig. S2). Upon the loading of the dual-atom Pt precursor, neither Pt nanoparticles nor nanoclusters were observed in the TEM (Supplementary Fig. S3) and HAADF-STEM images (Fig. 1a). Moreover, no additional diffraction peaks of Pt lattices were found in the XRD pattern (Supplementary Fig. S1). The energy-dispersive X-ray (EDX) spectroscopy further demonstrated a homogeneous distribution of the Pt species (Fig. 1b). The inductively coupled plasma optical emission spectrometry indicated that the content of Pt is 0.15 wt%. All the above results indicated that dual-atom Pt had been homogeneously dispersed on the mpg-C_3N_4 substrate. After the pyrolysis procedure, no infrared spectroscopy absorption peaks that correspond to the ligands of the precursor were observed in the Pt_2/mpg-C_3N_4 sample, which supported a complete removal of the ligand molecules (Supplementary Fig. S4). To further confirm the dual-atomic feature of the Pt species, aberration-corrected (AC) HAADF-STEM was applied to characterize the Pt_2/mpg-C_3N_4 sample. Many paired bright dots (marked with white circles) were observed in the AC HAADF-STEM image, which is consistent with the feature of two Pt atoms (Supplementary Fig. 1c). Besides, a few isolated bright dots (marked with green circles) were also observed, which we attributed to an overlap of paired Pt dots in the incident beam direction or an incomplete imaging of the dual-atom Pt species due to incomplete focusing (Supplementary Fig. 1c). The detailed features of Pt_2 dual-atom are different from each other depending on their orientations in three dimensions because the AC STEM image just showed a two-dimensional projection from the three-dimensional Pt_2/mpg-C_3N_4 samples.[47] For comparison, only isolated bright dots

appeared in the corresponding Pt_1/mpg-C_3N_4 image, further confirming the sharply difference between dual-atom and single-atom Pt species. (Fig. 1d and Supplementary Fig. S5-7).

X-ray absorption fine structure spectroscopy, which is a powerful technique for determining the chemical state and coordinated environment, was also applied to characterize the Pt species. The Pt L_3-edge X-ray absorption near-edge structure (XANES) spectra of the Pt_2/mpg-C_3N_4 and Pt_1/mpg-C_3N_4 samples, as well as the corresponding references, are shown in Fig. 2a. Here, the white line intensity peak of dual-atom Pt_2 is located between those of Pt foil and PtO_2, indicating that the two Pt atoms possess positive charges. This can be attributed to the strong interaction between the dual-atom Pt species and the mpg-C_3N_4 substrate or partial oxidation of dual-atom Pt by the O_2, which is similar to the case of Pt_1/mpg-C_3N_4. The Fourier-transformed (FT) k^3-weighted extended X-ray absorption fine structure (EXAFS) spectra of Pt_2/mpg-C_3N_4 showed a sharp peak located at 1.62 Å, which is also similar to the result of Pt_1/mpg-C_3N_4 and can be assigned to the Pt-N/O contributions (Fig. 2b). For Pt_2/mpg-C_3N_4, another distinct peak at 2.44 Å was found, similar to the Pt-Pt path of Pt foil but not observed in the spectrum of the Pt_1/mpg-C_3N_4 sample. It reveals that the Pt-Pt path should also be taken into account in the spectrum of Pt_2/mpg-C_3N_4. Wavelet Transforms (WT) EXAFS analysis is powerful method to discern the scattering atoms because it can provide both R-space and k-space resolutions. WT EXAFS analysis results show that the WT EXAFS spectrum of dual-atom Pt_2 shows maximum at 4.6 $Å^{-1}$ in k-space and 1.6 Å in R-space, corresponding to the Pt-O and Pt-N bond. Besides, two distinct peaks are observed at ~ 2.5 Å in R-space, which refers to the Pt-O (oxygen at second shell, k = 3.7 $Å^{-1}$) and Pt-Pt (k = 8 $Å^{-1}$). Therefore, the structure of Pt_2 consists of a Pt-Pt bond with surrounding O attached (Supplementary Fig. 2e). The EXAFS fitting results further showed that the first peak at 1.62 Å comes from the Pt–N/O contributions and the second one at 2.44 Å is from the Pt-Pt path (Fig. 2c-2d, Supplementary Fig. S8-9, and Supplementary Table 1). The coordination number of the Pt–N/O path was estimated to be 2.4 at the distances of 2.02 Å, and the second coordination sphere by the Pt-Pt path was assessed to 1.1 with the corresponding distance to be 2.61 Å.

The configuration of the Pt_2/mpg-C_3N_4 sample was also explored by extensive first-principles calculations, with the optimized geometry shown in the inset of Fig. 2c. Firstly, we considered various kinds of Pt_2/g-C_3N_4 structures without oxygen atoms (Supplementary Fig. S10) in the simulations, but none of them matched the XAFS information. It is worth noting that, since the measurement of the XAFS spectra were performed in air, the oxygen molecules contained in the atmosphere had interacted with and attached to the Pt species, which is also consistent with the WT EXAFS analysis result (Supplementary Fig. 2e). Such oxygen atoms, however, will be removed by hydrogen molecules at the initial stage of the following hydrogenation reaction. Furthermore, we explored the possibility structures of dual-atom Pt_2 with the oxygen atoms (Fig. 2f and Supplementary Fig. S11). Fortunately, the Pt-N/O and the Pt-Pt bond lengths were calculated to be 1.96 ± 0.14 Å and 2.55 Å, with the corresponding coordination numbers being 2.5 and 1.0 based on the model in Fig. 2c. The information agrees well with results from the XAFS data.

Hydrogenation of nitrobenzene to aniline. The catalytic performance of Pt_2/mpg-C_3N_4, Pt_1/mpg-C_3N_4, and Pt nanoparticles (~ 2 nm)/mpg-C_3N_4 (Supplementary Fig. S12) were then investigated. Under the conditions of 4 MPa H_2 pressure and 100°C, a conversion of ≥99% was obtained on the Pt_2/mpg-C_3N_4 catalyst for the hydrogenation of nitrobenzene to aniline, while no by-product was detected (Fig. 3a). Such Pt_2/mpg-C_3N_4 sample can be reused at least five times without any loss of the activity (Fig. 3b). After five cycles, the HAADF-STEM image and EXAFS spectrum of the Pt_2/mpg-C_3N_4 material did not exhibit any change, indicating that the Pt species were still well dispersed as dual-atom Pt pairs (Supplementary Fig. S13-14). It may be worth mentioning that the mpg-C_3N_4 support is reactively inert under the same conditions. By contrast, the corresponding conversions of Pt_1/mpg-C_3N_4 and Pt nanoparticles/mpg-C_3N_4 sharply dropped to 23% and 12%, respectively, demonstrating the uniqueness of the dual-atom Pt species in the catalytic properties (Fig. 3a). To investigate whether the outstanding catalytic performance is general for the hydrogenation of nitroarenes, we have explored the hydrogenation of several other nitroarene derivatives, including p-nitrophenol, p-nitrotoluene, tetrachloro-nitrobenzene, and tetrabromonitrobenzene. We found that Pt_2/mpg-C_3N_4 exhibits excellent yields for all corresponding anilines (Fig. 3c).

The superior catalytic performance of Pt_2/mpg-C_3N_4 compared with those of the Pt_1/mpg-C_3N_4 sample and the Pt nanoparticles was, according to our first-principles simulations, attributed to the formation of the Pt-O chemical bonds between the diatomic Pt_2 species and the nitro groups, which brings about effective activation of the N-O bonds. In Fig. 4, we present the adsorption configurations of nitrobenzene on Pt_2/g-C_3N_4 and Pt_1/g-C_3N_4 as well as on a Pt(111) surface (to represent the outermost layer of Pt nanoparticles). One can see that on Pt_2/g-C_3N_4, the two oxygen atoms of the nitro group can form chemical bonds with the two Pt atoms, while on Pt_1/g-C_3N_4 and Pt(111), the nitro group becomes far away from the Pt atoms. Only in the former case, the N-O bond lengths exhibit a significant elongation from 1.25 Å (the corresponding value of an isolated nitrobenzene molecule) to 1.35 Å, which makes the N-O bond rupture become much easier in the subsequent hydrogenations.

In the reduction of nitrobenzene to aniline, the detailed processes of the N-O bond cleavage and the N-H bond formation are displayed in Fig. 5. As we have expected based on the elongation of the N-O bonds, the N-O rupture is easy to occur (S2), during which a barrier of only 0.60 eV (TS1) is required to overcome. After that, the first H_2 molecule approaches the N and the O atoms (S3) and reacts with them via the Eley–Rideal (ER) mechanism (TS2), producing the first N-H bond and a hydroxyl group (S4). Upon the elimination of the hydroxyl group by a second H_2 molecule (not shown in Fig. 5), the second N-O bond is broken in the same way (S6), showing a barrier of 0.61 eV (TS3). As the third H_2 molecule participates in the reaction through the same ER mechanism (S7 and TS4), the second N-H bond is formed, corresponding to the production of aniline (S8). After desorption of the aniline product and recombination of the remaining hydroxyl group and H atom, as well as adsorption of another nitrobenzene molecule (S1), a new round of the catalytic cycle will start again.

Hydrogenation of benzaldehyde and epoxidation of alkenes.

The produced Pt_2/mpg-C_3N_4 catalyst is versatile and can be employed in other important reactions besides the selective hydrogenation of nitrobenzene. For example, under the conditions of 4 MPa H_2 pressure and 120°C, the Pt_2/mpg-C_3N_4 sample showed optimal catalytic performance toward the hydrogenation of benzaldehyde to benzyl alcohol (Fig. 6a). Specifically, ~99% conversion and ~99% selectivity were achieved for 7 hours. It means that the aforementioned activation pattern of Pt_2 can be extended to activating substituted C = O bonds near benzene rings (Supplementary Fig. 15). Moreover, the catalyst can be reused at least three times without any loss of the activity (Fig. 6a). As another type of significantly important reactions,[48] the epoxidation of alkenes in liquid relies on extensive use of expensive oxidants or co-reagents, which leads to a large increase in the cost. Our prepared Pt_2/mpg-C_3N_4 catalyst exhibited excellent catalytic performance toward the epoxidation of styrene when only O_2 molecules were used as the oxidant, which well circumvents the above problem. In Fig. 6b, one can see that Pt_2/mpg-C_3N_4 exhibited a conversion of 93% and a selectivity of 78% after 12 h, and this is one of the best results for the epoxidation of styrene.[49–50] Here, the one-coordinated oxygen atom on the Pt_2 species (Fig. 2f) plays an important role in the catalytic reaction, which is reminiscent of the diatomic Fe_2 system in catalyzing the epoxidation of *trans*-stilbene.[26]

Discussion

In conclusion, we have reported an atomically monodispersed dual-atom Pt heterogeneous catalyst, which exhibited excellent catalytic properties in selective hydrogenation and epoxidation reactions. Multiple characterization techniques, including aberration-corrected STEM, XAFS spectra, and first-principles simulations, were employed to capture the structural and chemical nature of the dual-atom Pt species. Compared with the mpg-C_3N_4-supported Pt single-atom catalysts and ultra-small Pt nanoparticles, Pt_2/mpg-C_3N_4 exhibited much better performance toward the selective hydrogenation of nitrobenzene, which originates from an effective activation of the N = O bonds by the Pt_2 species. More interestingly, the prepared Pt_2/mpg-C_3N_4 catalyst is versatile and can be applied in catalyzing other important reactions, like the hydrogenation of aldehyde compounds and the epoxidation of alkenes.

Materials And Methods

Materials

Cyanamide (98%), LUDOXR AS-40 colloidal silica 40 wt% suspension in H_2O, Ammonium hydrogen difluoride, Hydrogen hexachloroplatinate(IV) hydrate, Platinum(II) 2,4-pentanedionate and (Ethylenediamine)iodoplatinum(II) dimer dinitrate were purchased from Innochem. Ethanol, N,N-dimethylformamide, and n-hexane were purchased from Sinopharm Chemical Reagent Co. Ltd. Oleylamine and borane-tert-butylamine were purchased from Sigma-Aldrich Reagent Company.

Synthesis of mpg-C_3N_4, and Pt nanoparticles.

The synthesis of mpg-C_3N_4 was according to the previous method without any changing.[46] In preparation of Pt nanoparticles, 20 mg Pt(II) acetylacetonate was dissolved in 10 mL OAm at 120 ℃. Then, a solution of 100 mg borane-tert-butylamine in 2 mL OAm was added quickly into the previous solution. After 2 min, the flask was heated to 140 ℃ for a further 1 hour. After cooling to room temperature, the solution was washed with ethanol.

Synthesis of Pt_2/mpg-C_3N_4, Pt_1/mpg-C_3N_4, and Pt NPs/mpg-C_3N_4.

In the typical synthesis of Pt_2/mpg-C_3N_4, 500 mg mpg-C_3N_4 and 5 mg (Ethylenediamine)iodoplatinum(II) dimer dinitrate were dissolved in the 100 mL DMF under the stirring condition. After continuous stirring about 12h, the suspension was centrifuged. The obtained solid was washed with DMF and methanol. The as-prepared powder was treated under the N_2 atmosphere at 300 °C for 2 hours. The loading of Pt, determined by ICP-OES analysis, is 0.15 wt%. When the temperature is above 300 °C, thermogravimetric analysis (TGA) showed almost no more weight was losing, which indicated the ligand is removed completely (**Fig. S16**). The synthesis methods of Pt_1/mpg-C_3N_4 and Pt nanoparticles/mpg-C_3N_4 are similar to the Pt_2/mpg-C_3N_4 with some changing. In the synthesis of Pt_1/mpg-C_3N_4, 500 mg mpg-C_3N_4 was dissolved in the 100 mL H_2O. Then, The 2.5 mg H_2PtCl_6 in 10 mL H_2O was added to the above solution under vigorous stirring. After continuous stirring about 12h, the suspension was centrifuged. The as-prepared powder was treated under the N_2 atmosphere at 125 °C for 2 hours. The loading of Pt, determined by ICP-OES analysis, is 0.18 wt%. In the synthesis of Pt nanoparticles/mpg-C_3N_4, 5 mg Pt nanoparticles and 500mg mpg-C_3N_4 were dissolved in the mixture of 100 mL ethanol and 100 mL n-hexane under stirring at room temperature for 12 hours. The product was separated by centrifugation, then washed with methanol. The as-prepared powder was treated under the N_2 atmosphere at 125 °C for 2 hours. The Pt loading is 0.42% determined by ICP-OES analysis.

Catalytic tests

Typical procedure for the hydrogenation of nitro-compound. In the typical experiment, the reaction mixture containing 1 mmol nitrocompound, catalyst {equal 0.000373 mmol Pt for Pt_1/mpg-C_3N_4, Pt_2/mpg-C_3N_4 and Pt nanoparticles/mpg-C_3N_4 or 50 mg mpg-C_3N_4} and 10 mL isopropanol were loaded into the reactor. The reactor was sealed then pressurized with 1 MPa H_2 and 3 MPa N_2 to a setting point. The reaction was then heated to the 100 ℃ and kept for 3 hours. The products were identified by GC-MS and GC.

Following the hydrogenation reaction, the reaction mixture was centrifuged to recover the catalyst, which was washed first with acetone then water followed by drying under vacuum oven at 50 ^{o}C and employed for the next catalytic test.

Typical procedure for the hydrogenation of benzaldehyde. In the typical experiment, the reaction mixture containing benzaldehyde (1 mmol), 50mg Pt_2/mpg-C_3N_4 and 10 mL isopropanol were loaded into the reactor. The reactor was sealed, purged three times with N_2 at 1 MPa and then pressurized with 4 MPa H_2 and 4 MPa N_2 to a setting point. The reaction was then heated to the 120 °C temperature and kept for 9 hours.

Typical procedure for the epoxidation of styrene. 1 mmol styrene, 20 mg Pt_2/mpg-C_3N_4 and 5 mL 1,4-dioxane were mixed in a 20 ml of Schleck tube. Then, the air in the tube was removed by the oil pump. An O_2 balloon was used to blow about 1 atm O_2. Finally, the reaction vessel was heated in a oil bath at 100 ^oC for 12 hours.

Characterization

XAFS measurements and analysis. The XAFS data of Pt L_3-edge was collected in fluorescence excitation mode using a Lytle detector at 1W1B station in Beijing Synchrotron Radiation Facility. The EXAFS data were processed by the standard procedures using the ATHENA module implemented in the IFEFFIT software packages. To obtain the quantitative structural parameters around central atoms, the least-squares curve parameter fitting was performed using the ARTEMIS module of IFEFFIT software packages.

Details of calculations. All the calculations were conducted using the Vienna *ab initio* simulation package.[51-52] The projector augmented wave approach[53] was employed, and the energy cutoff of the plane-wave basis set was set to 500 eV. The exchange-correlation interactions were described by the optPBE-vdW functional,[54-55] which explicitly includes effects of van der Waals forces. The first Brillouin zone was sampled using a 3×3×1 Monkhorst-Pack grid.[56] To simulate the mpg-C_3N_4 and the Pt nanoparticles, a g-C_3N_4 monolayer and a Pt(111) slab model (four layers with sixteen Pt atoms within each layer) were employed, respectively. Structural relaxations were performed until the maximum residual force on each atom was less than 0.03 eV/Å. Transition states were located using the climbing-image nudged elastic band method[57] with a force criterion of 0.10 eV/Å. A dipole correction to the total energies was applied along the vertical direction.

Declarations

Data availability. The data supporting this study are available from the authors upon reasonable request.

Acknowledgments

This work was supported by the National Key R&D Program of China (2018YFA0702003) and the National Natural Science Foundation of China (21890383, 21671117, 21871159, and 21803036). Q.F. also thanks the Shandong Provincial Natural Science Foundation, China (ZR2018QB005) and the Young Scholars Program of Shandong University (2018WLJH49). First-principles calculations were performed

on the HPC Cloud Platform of Shandong University and the super-computing system in Shanghai-SCC. We thank the 1W1B station in Beijing Synchrotron Radiation Facility.

Author contributions

S.T. conducted and designed the experiments, analyzed the data and wrote the paper. Z. H. and Q.F. Y.B. conducted the DFT calculations. H.Z. designed the hydrogenation reaction. W.G, and C.C did the hydrogenation reaction and analyzed the data. Q.X, W.C, Y.Z., J.Y., and X.S helped to analyze the data. D.W. and Y.L. conceived and designed the research project. All authors contributed to the preparation of the manuscript.

Competing financial interests

The authors declare no competing interests.

Additional Information

Supplementary Information accompanies this paper at

http://www.nature.com/naturecommunications

Reprints and permission information is available online at

http://npg.nature.com/reprintsandpermissions/

How to cite this article:

References

1. Kaden, W. E. Wu, T. Kunkel, W. A. & Anderson, S. L. Electronic Structure Controls Reactivity of Size-Selected Pd Clusters Adsorbed on TiO_2 Surfaces. *Science* **326**, 826-829 (2009).
2. Bonanni, S. Ait-Mansour, K. Harbich, W. & Brune, H. Effect of the TiO_2 Reduction State on the Catalytic CO Oxidation on Deposited Size-Selected Pt Clusters. *J. Am. Chem. Soc.* **134**, 3445-3450 (2012).
3. Okrut, A. et al. Selective Molecular Recognition by Nanoscale Environments in a Supported Iridium Cluster Catalyst. *Nat. Nanotechnol.* **9**, 459-465 (2014).
4. Liu, L. & Corma, A. Metal catalysts for heterogeneous catalysis: from single atoms to nanoclusters and nanoparticles. *Chem. Rev.* **118**, 4981-5079 (2018).
5. Yoon, B. et al. Charging effects on Bonding and Catalyzed Oxidation of CO on Au_8 Clusters on MgO. *Science* **307**, 403-407 (2005).
6. Liu, C. et al. Carbon Dioxide Conversion to Methanol over Size-Selected Cu_4 Clusters at Low Pressures. *J. Am. Chem. Soc.* **137**, 8676-8679 (2015).

7. Liu, J. C. et al. Heterogeneous Fe_3 Single-Cluster Catalyst for Ammonia Synthesis Via an Associative Mechanism. *Nat. Commun.* **9**, 1610 (2018).
8. Ye, W. et al. Precisely Tuning the Number of Fe Atoms in Clusters on N-Doped Carbon toward Acidic Oxygen Reduction Reaction. *Chem* **5**, 2865-2878 (2019).
9. Ren, W. et al. Isolated Diatomic Ni-Fe Metal–Nitrogen Sites for Synergistic Electroreduction of CO_2. *Angew. Chem. Int. Ed.* 58, 6972-6976 (2019).
10. Liu, J. et al. Tackling CO Poisoning with Single-Atom Alloy Catalysts. *J. Am. Chem. Soc.* **138**, 6396-6399 (2016).
11. Moliner, M.; et al. Reversible Transformation of Pt Nanoparticles into Single Atoms inside High-Silica Chabazite Zeolite. *J. Am. Chem. Soc.* **138**, 15743-15750 (2016).
12. Zhang, H. et al. Efficient Visible-Light-Driven Carbon Dioxide Reduction by a Single-Atom Implanted Metal-Organic Framework. *Angew. Chem. Int. Ed.* 55, 14310-14314 (2016).
13. Malta, G. et al. Identification of Single-Site Gold Catalysis in Acetylene Hydrochlorination. *Science* **355**, 1399-1403 (2017).
14. Huang, F. et al. Atomically Dispersed Pd on Nanodiamond/Graphene Hybrid for Selective Hydrogenation of Acetylene. *J. Am. Chem. Soc.* **140**, 13142-13146 (2018).
15. Li, T. et al. Maximizing the Number of Interfacial Sites in Single-Atom Catalysts for the Highly Selective, Solvent-Free Oxidation of Primary Alcohols. *Angew. Chem. Int. Ed.* **57**, 7795-7799 (2018).
16. Qin, R. X. Liu, P. X. Fu, G. & Zheng, N. F., Strategies for Stabilizing Atomically Dispersed Metal Catalysts. *Small Methods* **2**, 1700286 (2018).
17. Abdel-Mageed, A. M. Rungtaweevoranit, B. Parlinska-Wojtan, M. Pei, X. Yaghi, O. M. & Behm, R. J. Highly Active and Stable Single-Atom Cu Catalysts Supported by a Metal-Organic Framework. *J. Am. Chem. Soc.* 141, 5201-5210 (2019).
18. Cao, L. et al. Atomically Dispersed Iron Hydroxide Anchored on Pt for Preferential Oxidation of CO in H_2. *Nature* 565, 631-635 (2019).
19. Lee, B. H. et al. Reversible and Cooperative Photoactivation of Single-Atom Cu/TiO_2 Photocatalysts. *Nat. Mater.* 18, 620-626 (2019).
20. Tang, Y. et al. Synergy of Single-Atom Ni_1 and Ru_1 Sites on CeO_2 for Dry Reforming of CH_4. *J. Am. Chem. Soc.* **141**, 7283-7293 (2019).
21. Zhuang, Z. Kang, Q. Wang, D. & Li, Y., Single-atom Catalysis enables Long-Life, High-Energy Lithium-Sulfur Batteries. *Nano Res.* 2020, DOI: org/10.1007/s12274-020-2827-4.
22. Xu, Q. et al. Coordination Structure Dominated Performance of Single-Atomic Pt Catalyst for Anti-Markovnikov Hydroboration of Alkenes. *Sci. China Mater.* **63**, 972-981 (2020).
23. Li, X. Rong, H. Zhang, J. Wang, D. & Li Y. Modulating the Local Coordination Environment of Single-Atom Catalysts for Enhanced Catalytic Performance. *Nano Res.* 2020, DOI: org/10.1007/s12274-020-2755-3.

24. He, Z. et al. Atomic Structure and Dynamics of Metal Dopant Pairs in Graphene. *Nano Lett.* **14**, 3766-3772 (2014).
25. Mon, M. et al. Synthesis of Densely Packaged, Ultrasmall Pt^0_2 Clusters within a Thioether-Functionalized MOF: Catalytic Activity in Industrial Reactions at Low Temperature. *Angew. Chem. Int. Ed.* 57, 6186-6191 (2018).
26. Tian, S. et al. Carbon Nitride Supported Fe_2 Cluster Catalysts with Superior Performance for Alkene Epoxidation. *Nat. Commun.* **9**, 2353 (2018).
27. Vorobyeva, E. et al. Atom-by-Atom Resolution of Structure-Function Relations over Low-Nuclearity Metal Catalysts. *Angew. Chem. Int. Ed.* 58, 8724-8729 (2019).
28. Yan, H. et al. Bottom-up Precise Synthesis of Stable Platinum Dimers on Graphene. *Nat. Commun.* 8, 1070 (2017).
29. Li, H. et al. Synergetic Interaction Between Neighbouring Platinum Monomers in CO_2 Hydrogenation. *Nat. Nanotechnol.* 13, 411-417 (2018).
30. Zhao, Y. et al. Stable Iridium Dinuclear Heterogeneous Catalysts Supported on Metal-Oxide Substrate for Solar Water Oxidation. *Proc. Natl. Acad. Sci. U S A* 115, 2902-2907 (2018).
31. Han, X.; et al. Atomically Dispersed Binary Co-Ni Sites in Nitrogen-Doped Hollow Carbon Nanocubes for Reversible Oxygen Reduction and Evolution. *Adv. Mater.* **31**, e1905622 (2019).
32. Zhang, L. et al. Atomic Layer Deposited Pt-Ru Dual-Metal Dimers and Identifying Their Active Sites for Hydrogen Evolution Reaction. *Nat. Commun.* **10**, 4936 (2019).
33. Yang, Y. et al. O-coordinated W-Mo Dual-atom Catalyst for pH-universal Electrocatalytic Hydrogen Evolution. *Sci. Adv.* **6**, eaba6586 (2020).
34. Lane, B. S. & Burgess, K. Metal-catalyzed Epoxidations of Alkenes with Hydrogen Peroxide. *Chem. Rev.* **103**, 2457-2473 (2003).
35. Vile, G. Albani, D. Almora-Barrios, N. Lopez, N. & Perez-Ramirez, J. Advances in the Design of Nanostructured Catalysts for Selective Hydrogenation. *ChemCatChem* **8**, 21-33 (2016).
36. Corma, A. & Serna, P. Chemoselective Hydrogenation of Nitro Compounds with Supported Gold Catalysts. *Science* **313**, 332-334 (2006).
37. Blaser, H.-U. Steiner, H. & Studer, M., Selective Catalytic Hydrogenation of Functionalized Nitroarenes: An Update. *ChemCatChem* **1**, 210-221 (2009).
38. Liu, P. X. et al, Photochemical Route for Synthesizing Atomically Dispersed Palladium Catalysts. Science **352**, 797-801 (2016).
39. Zhao, M. T. et al. Metal-Organic Frameworks as Selectivity Regulators for Hydrogenation Reactions. *Nature* **539**, 76-80 (2016).
40. Kamata, K. Yonehara, K. Sumida, Y. Yamaguchi, K. Hikichi, S. & Mizuno, N. Efficient Epoxidation of Olefins with >= 99% Selectivity and Use of Hydrogen Peroxide. *Science* **300**, 964-966 (2003).
41. Hughes, M. D. et al. Tunable Gold catalysts for Selective Hydrocarbon Oxidation Under Mild Conditions. *Nature* **437**, 1132-1135 (2005).

42. McGarrigle, E. M. & Gilheany, D. G., Chromium- and Manganese-salen Promoted Epoxidation of Alkenes. *Chem. Rev.* **105**, 1563-1602 (2005).
43. Bauer, I. & Knolker, H. J. Iron Catalysis in Organic Synthesis. *Chem. Rev.* **115**, 3170-387 (2015).
44. Nie, R. Wang, J. Wang, L. Qin, Y. Chen, P. & Hou, Z. Platinum Supported on Reduced Graphene Oxide as a Catalyst for Hydrogenation of Nitroarenes. *Carbon* **50**, 586-596 (2012).
45. Xiang, Q. Yu, J. & Jaroniec, M. Preparation and Enhanced Visible-Light Photocatalytic H2-Production Activity of Graphene/C3N4 Composites. *J. Phys. Chem. C* **115**, 7355 (2011).
46. Goettmann, F.; Fischer, A.; Antonietti, M.; Thomas, A. Chemical synthesis of mesoporous carbon nitrides using hard templates and their use as a metal-free catalyst for Friedel–Crafts reaction of benzene. *Angew. Chem., Int. Ed.* **45**, 4467 (2006).
47. Li, Z. Y. et al. Three-dimensional Atomic-scale Structure of Size-selected Gold Nanoclusters. *Nature* 451, 46-48 (2008).
48. Hughes, M. D. et al. Tunable gold catalysts for selective hydrocarbon oxidation under mild conditions. *Nature* 437, 1132-1135 (2015).
49. Turner, M. et al. Selective Oxidation with Dioxygen by Gold Nanoparticle Catalysts Derived from 55-atom Clusters. *Nature* 454, 981-983 (2008).
50. Qian, L. et al. Stable and Solubilized Active Au Atom Clusters for Selective Epoxidation of Cis-cyclooctene with Molecular Oxygen. *Nat. Commun.* **8**, 14881 (2017).
51. Kresse, G. & Furthmüller, J. Efficiency of ab-initio total energy calculations for metals and semiconductors using a plane-wave basis set. *Comput. Mater. Sci.* **6**, 15-50 (1996).
52. Kresse, G. & Furthmüller, J. Efficient iterative schemes for ab initio total-energy calculations using a plane-wave basis set. *Phys. Rev. B* **54**, 11169-11186 (1996).
53. Blöchl, P. E. The projector augmented wave method, *Phys. Rev. B* **50**, 17953-17979 (1994).
54. Dion, M. Rydberg, H. Schröder, E. Langreth, D. C. & Lundqvist, B. I. Van der waals density functional for general geometries. *Phys. Rev. Lett.* **92**, 246401 (2004).
55. Klimeš, J. Bowler, D. R. & Michaelides, A. Chemical accuracy for the van der waals density functional. *J. Phys.:Condens. Matter.* **22**, 022201 (2010).
56. Monkhorst, H. J. & Pack, J. D. Special points for brillouin-zone integrations. *Phys. Rev. B* **13**, 5188-5192 (1976).
57. Henkelman, G. Uberuaga, B. P. & Jónsson, H. A climbing image nudged elastic band method for finding saddle points and minimum energy paths. *J. Chem. Phys.* **113**, 9901-9904 (2000).

Figures

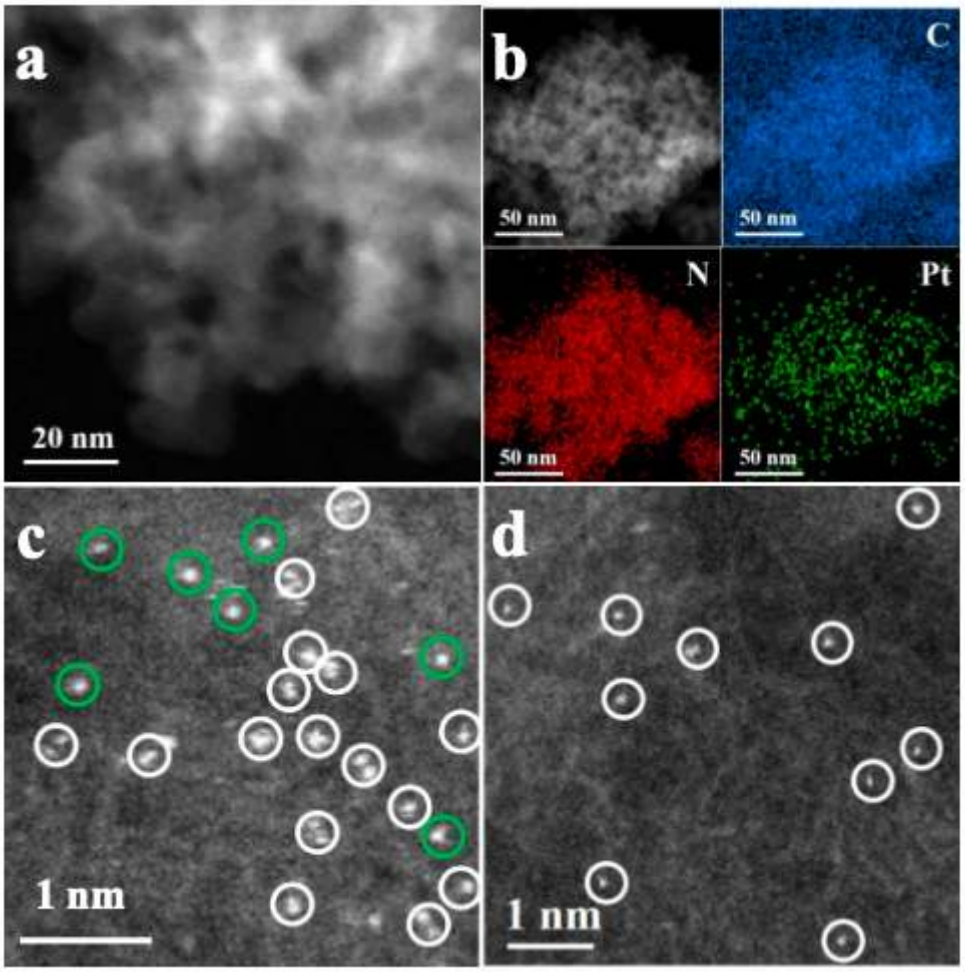

Figure 1

Characterization of Pt2/mpg-C3N4 sample. (a) HAADF-STEM image of Pt2/mpg-C3N4. (b) EDX mapping distributions of the C (blue), N (red), and Pt (green) elements, respectively. (c, d) AC HAADF-STEM images of the Pt2/mpg-C3N4 and Pt1/mpg-C3N4 samples, respectively.

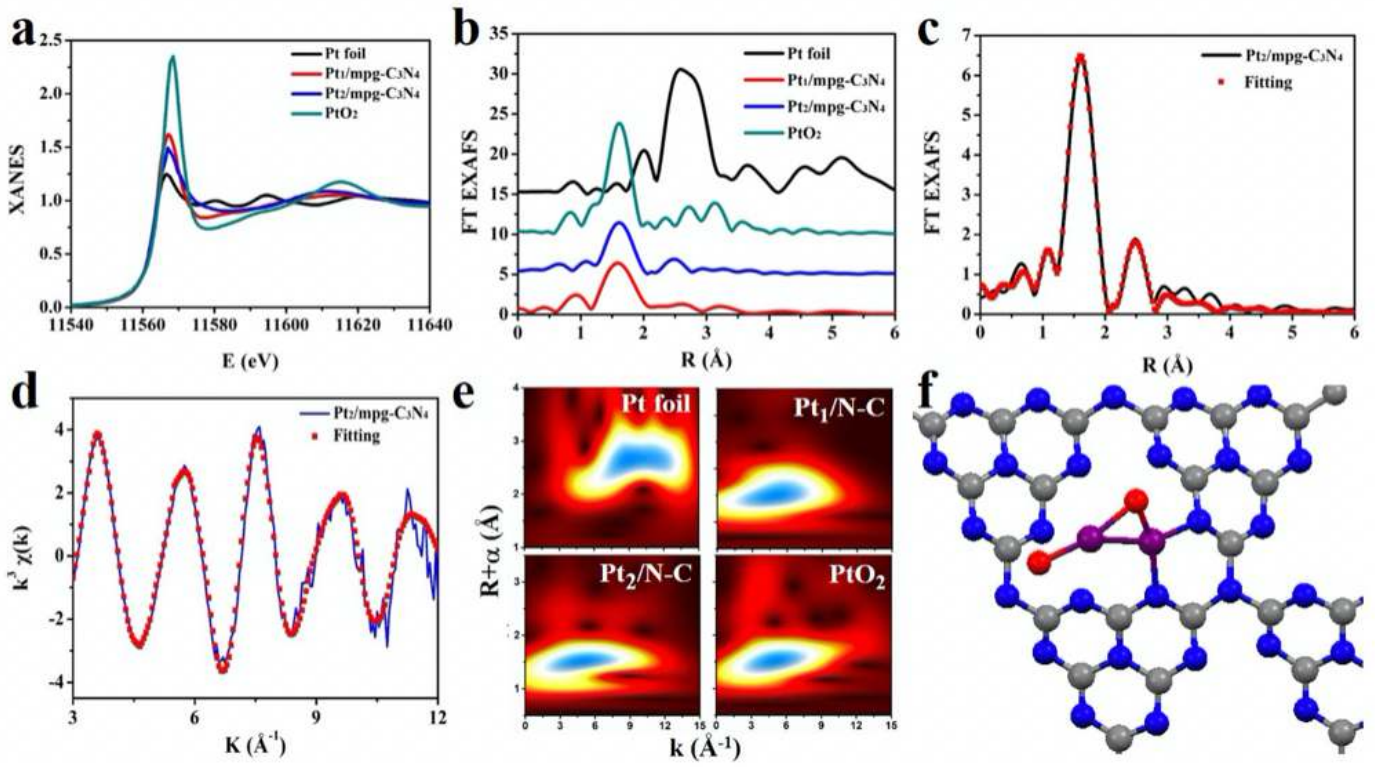

Figure 2

Pt L3-edge XAFS analysis. (a, b) XANES and FT EXAFS spectra of Pt2/mpg-C3N4, Pt1/mpg-C3N4, and corresponding references. (c, d) The FT EXAFS fitting spectrum of Pt2/mpg-C3N4 at R and K space, respectively. The inset of c is the optimized geometry of Pt2/mpg-C3N4. (e) WT EXAFS of Pt foil, Pt1/mpg-C3N4, Pt2/mpg-C3N4, and PtO2. (f) The schematic model of Pt2/mpg-C3N4 (C: grey; N: blue; O: red; Pt: purple).

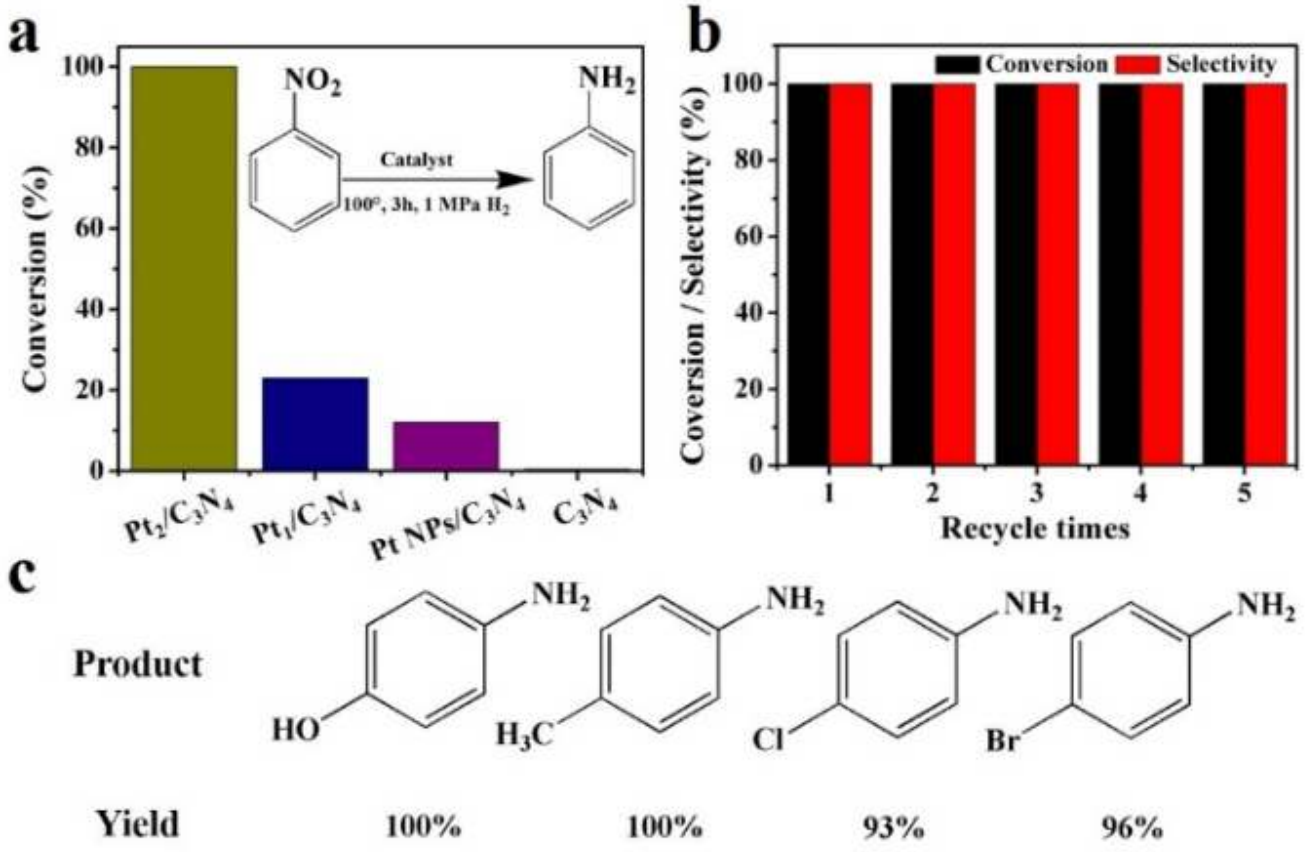

Figure 3

Hydrogenation of nitrobenzene. (a) Catalytic performance for the hydrogenation of nitrobenzene by Pt2/mpg-C3N4 and other reference samples. (b) Recycling of Pt2/mpg-C3N4 for the catalytic hydrogenation of nitrobenzene. (c) Hydrogenation of functionalized nitroarenes catalyzed by Pt2/mpg-C3N4.

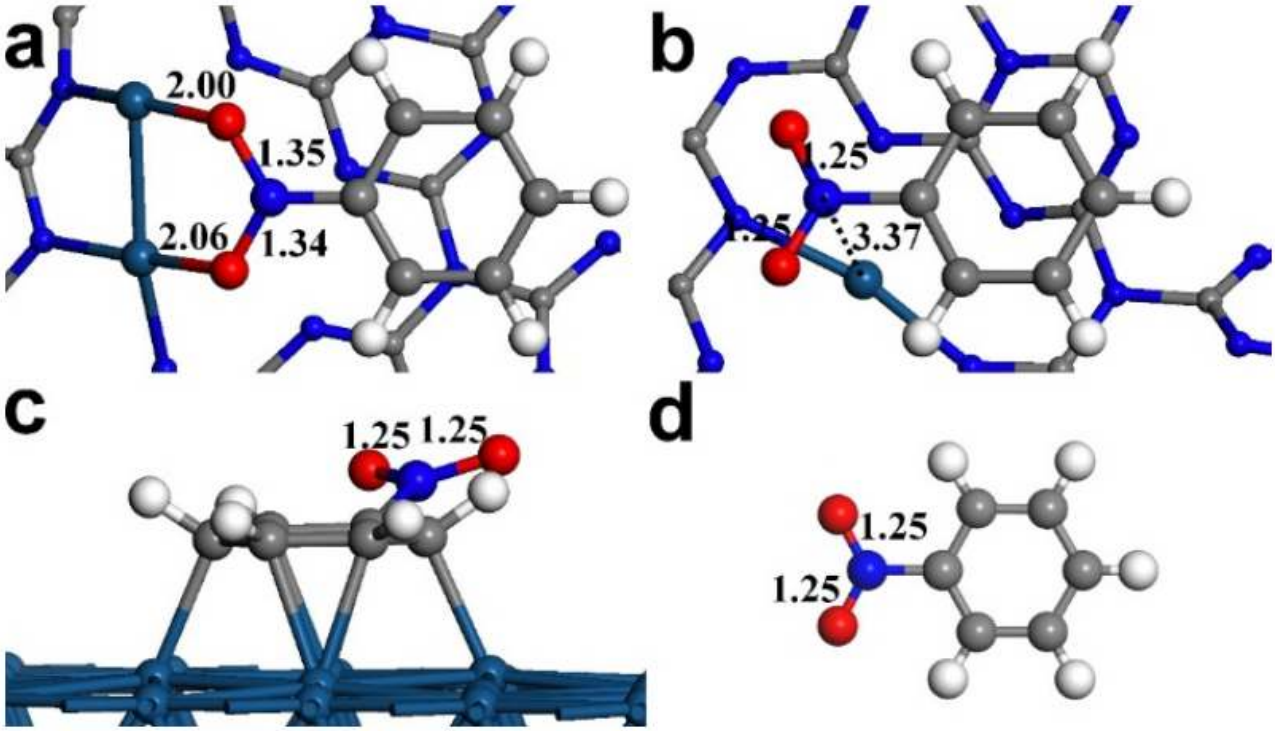

Figure 4

Configurations of an adsorbed nitrobenzene molecule. (a) On the Pt2/g-C3N4 and (b) the Pt1/g-C3N4 samples, as well as on (c) a Pt(111) surface. The geometry of isolated nitrobenzene is shown in (d). Bond lengths (in Å) are marked in black. The teal, gray, blue, red, and white spheres represent the Pt, C, N, O, and H atoms, respectively.

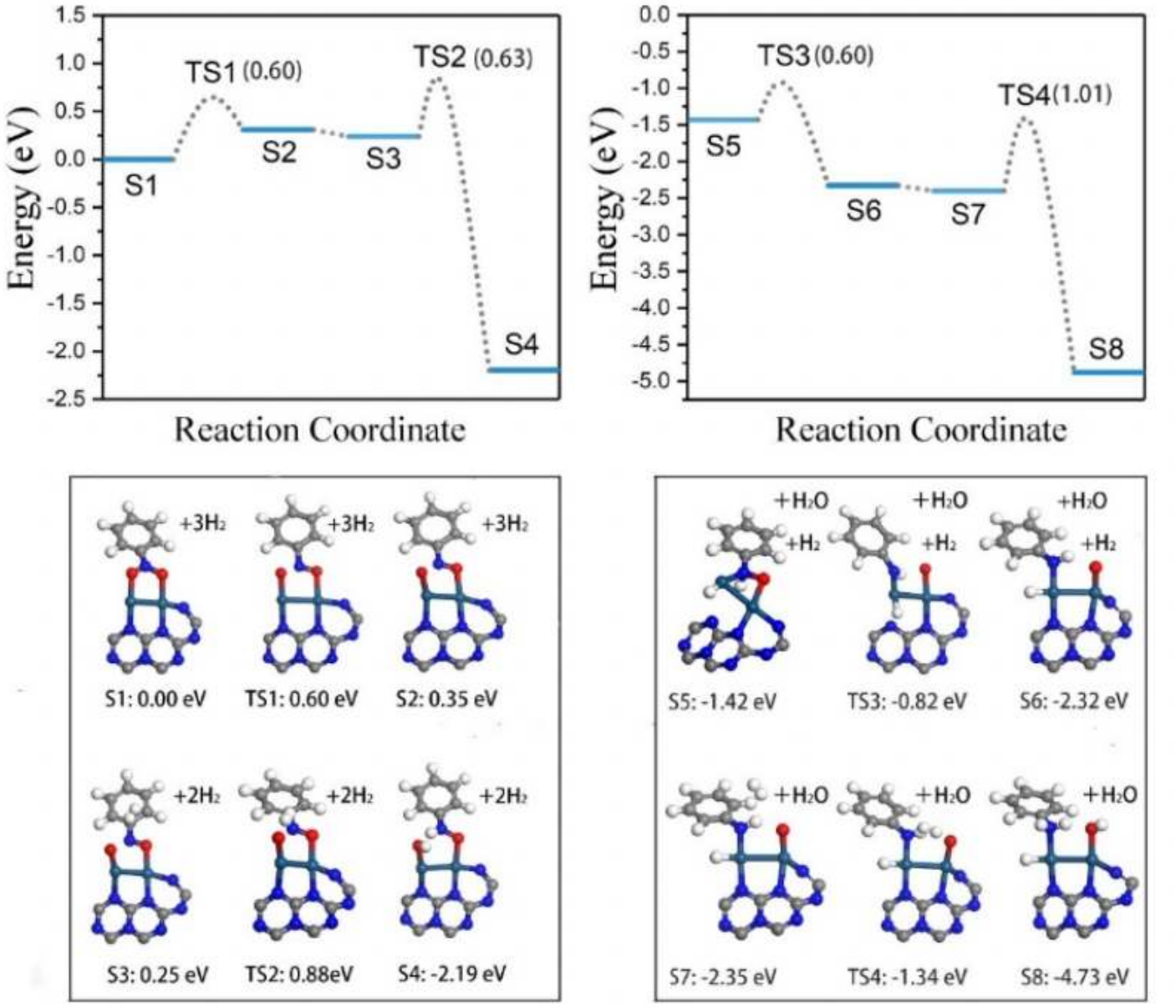

Figure 5

Reaction pathways of hydrogenation of nitrobenzene. Reaction pathways for the N-O bond cleavage and the N-H bond formation (left column: the first time; right column: the second time) in the reduction from nitrobenzene to aniline. The values of the energy barriers are listed within the parentheses in the top panels.

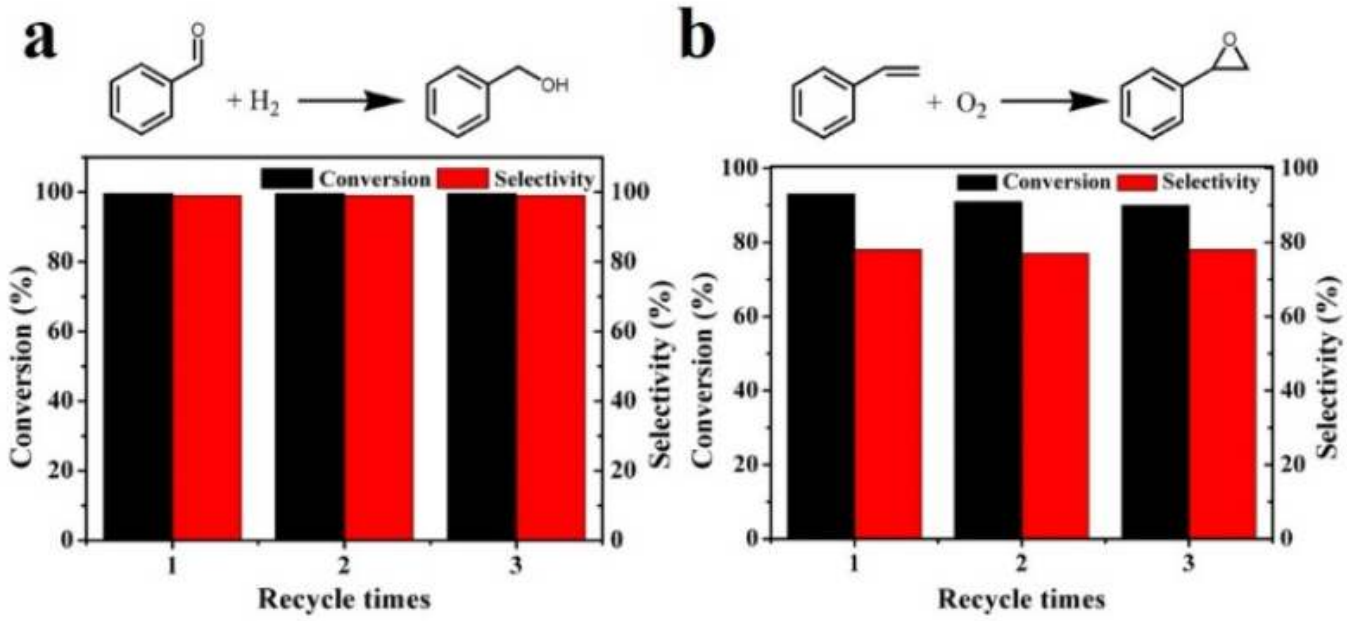

Figure 6

Hydrogenation of benzaldehyde and epoxidation of styrene. (a) Catalytic performance for the hhydrogenation of benzaldehyde by using the Pt2/mpg-C3N4 catalyst. (b) Corresponding catalytic performance for the epoxidation of styrene.

Supplementary Files

This is a list of supplementary files associated with this preprint. Click to download.

- SupplementaryInformation.pdf
- TOCgraphic.png